PCSK9 regulates the NODAL signaling pathway and cellular proliferation in hiPSCs

Meryl Roudaut, Salam Idriss, Amandine Caillaud, Aurore Girardeau, Antoine Rimbert, Benoite Champon, Amandine David, Antoine Lévêque, Lucie Arnaud, Matthieu Pichelin, et al.

PCSK9 regulates the NODAL signaling pathway and cellular proliferation in hiPSCs

Running title: PCSK9 function in hiPSCs

Meryl Roudaut[1,2#], Salam Idriss[1,3#], Amandine Caillaud[1], Aurore Girardeau[1], Antoine Rimbert[1], Benoite Champon[1], Amandine David[1], Antoine Lévêque[1], Lucie Arnaud[1], Matthieu Pichelin[1,4], Xavier Prieur[1], Annik Prat[5], Nabil G Seidah[5], Kazem Zibara[3], Cedric Le May[1], Bertrand Cariou[1,4§,*], Karim Si-Tayeb[1,§,*]

1. Université de Nantes, CNRS, INSERM, l'institut du thorax, F-44000 Nantes, France.
2. HCS Pharma, Lille, France
3. ER045 - Laboratory of Stem Cells: Maintenance, Differentiation and Pathology, Biology Department, Faculty of Sciences, Lebanese University, Beirut, Lebanon
4. Université de Nantes, CHU Nantes, CNRS, INSERM, l'institut du thorax, F-44000 Nantes, France.
5. University of Montreal, Montreal, QC, Canada

# These authors contributed equally.
§ Co-senior author.

* Corresponding authors:
bertrand.cariou@univ-nantes.fr
karim.si-tayeb@univ-nantes.fr

SUMMARY

Proprotein convertase subtilisin kexin type 9 (PCSK9) is a key regulator of LDL cholesterol metabolism and the target of lipid-lowering drugs. PCSK9 is mainly expressed in hepatocytes. Here, we show that PCSK9 is highly expressed in undifferentiated human induced pluripotent stem cells (hiPSCs). PCSK9 inhibition in hiPSCs with the use of shRNA, CRISPR/cas9-mediated knockout or endogenous *PCSK9* loss-of-function mutation R104C/V114A unveiled its new role as a potential cell cycle regulator through the NODAL signaling pathway. In fact, PCSK9 inhibition leads to a decrease of SMAD2 phosphorylation and hiPSCs proliferation. Conversely, PCSK9 overexpression stimulates hiPSCs proliferation. PCSK9 can interfere with the NODAL pathway by regulating the expression of its endogenous inhibitor DACT2, which is involved in the TGFß-R1 lysosomal degradation. Using different PCSK9 constructs we show that PCSK9 interacts with DACT2 through its CHRD domain. Altogether these data highlight a new role of PCSK9 in cellular proliferation and development.

HIGHLIGHTS

- PCSK9 is highly expressed in undifferentiated hiPSCs
- PCSK9 regulates hiPS cell proliferation
- PCSK9 controls NODAL signaling and SMAD2 phosphorylation in hiPSCs
- PCSK9 controls TGFß-R1 expression potentially through its interaction with DACT2

INTRODUCTION

Proprotein convertase subtilisin kexin type 9 (PCSK9) is a master regulator of cholesterol homeostasis (for review, see (Seidah et al., 2017; Stoekenbroek et al., 2018)). PCSK9 was initially discovered as the third gene of familial hypercholesterolemia (FH), an autosomal co-dominant disorder that leads to premature atherosclerotic cardiovascular disease (Abifadel et al., 2003). While *PCSK9* gain-of-function (GOF) mutations cause FH, *PCSK9* loss-of-function (LOF) variants are conversely associated with reduced low-density lipoprotein (LDL) cholesterol levels and coronary heart disease (Cohen et al., 2006). Mendelian randomization studies further validate the concept that PCSK9 inhibition reduces cardiovascular events (Ference et al., 2016), leading to the development of PCSK9 inhibitors to manage cardiovascular disease in clinical practice (Preiss et al., 2020).

The canonical action of PCSK9 is to promote the downregulation of LDL receptor (LDLR) expression (Maxwell and Breslow, 2004). PCSK9 is mainly expressed in the hepatocyte, where it undergoes in the endoplasmic reticulum an autocatalytic cleavage between its pro and catalytic domains (Benjannet et al., 2004). One surprising key feature that distinguishes PCSK9 from the other proprotein convertases is that its prodomain is not released after its cleavage and remains closely bound in the catalytic site, leading to a secreted inactive protease (Seidah et al., 2003). After its cleavage, PCSK9 is secreted into the circulation, binds to the epidermal growth factor precursor homology domain A (EGF-A) extra-cellular domain of the LDLR and is internalized together with the receptor. The presence of the adaptor protein (LDLRAP1) that interacts intracellularly with the LDLR tail is required to allow the internalization of the LDLR-PCSK9 complex. Inside the cell, the binding of PCSK9 to the LDLR alters its acidic pH induced conformational change, which prevents normal recycling of the LDLR and instead targets the LDLR/PCSK9 complex to lysosomal degradation (Zhang et al., 2007). All the mechanistic steps by which this intracellular trafficking of the LDLR-PCSK9 complex takes place have not yet been fully elucidated (Seidah et al., 2017).

Beyond this so-called extracellular route of action of PCSK9, several data suggest that PCSK9 can act on the LDLR directly *via* an intracellular Golgi-lysosome route (Poirier et al., 2009). The existence of an intracellular route was supported by the fact that PCSK9 and the LDLR can interact very early inside the cell in the secretory pathway and more importantly that PCSK9 maintains its ability to promote LDLR degradation in cells devoid of LDLRAP1 protein (Poirier et al., 2009). PCSK9 inhibitors, alirocumab and evolocumab, are human monoclonal antibodies that interfere with the extra-cellular pathway by neutralizing

circulating PCSK9 and thus preventing its binding to the LDLR. Alternatively, inclisiran, a small interfering RNA which inhibits hepatic synthesis of PCSK9, impacts both extra-cellular and intra-cellular PCSK9 signaling pathways (Catapano et al., 2020).

We previously published that urine-sample-derived human induced pluripotent stem cells (hiPSCs) differentiated into hepatocyte-like cells (HLCs) is a relevant model to study the impact of *PCSK9* gain-of-function (GOF) and loss-of-function (LOF) mutations on cholesterol metabolism regulation (Si-Tayeb et al., 2016). During the validation process of our hiPSCs model, we made the intriguing observation that PCSK9 was highly expressed in undifferentiated hiPSCs, as previously noted (Assou et al., 2007; Calloni et al., 2013; Tsuneyoshi et al., 2008).

The aim of the present study is to decipher the function of PCSK9 in hiPSCs. By using both hiPSCs derived from patients with *PCSK9* LOF mutations and control hiPSCs with PCSK9 silencing, knockout or overexpression, we showed that PCSK9 interferes with the TGFβ-NODAL signaling pathway, a major actor in stem cells self-renewal, differentiation and proliferation (for review, see (Pauklin and Vallier, 2015)).

RESULTS

PCSK9 is highly expressed in undifferentiated hiPSCs

In order to gain further knowledge on the role of PCSK9 during hiPSCs hepatic differentiation, we monitored PCSK9 gene expression at each day throughout the procedure. As shown in **Figure 1A**, PCSK9 mRNA expression varies during hiPSCs differentiation. While PCSK9 expression has been already confirmed in HLCs (Si-Tayeb et al., 2016), we showed a stronger PCSK9 expression in the early stages of differentiation, such as the definitive endoderm and during its hepatic specification. Thereafter, hepatic differentiation upon HGF treatment (Days 11 to 15) induced a lower PCSK9 expression before a rebound during the final days of HLCs differentiation. In accordance with mRNA expression, PCSK9 protein expression (mature form (60kDa) and cleaved prodomain (15kDa)) was significantly higher in undifferentiated hiPSCs than in hepatic progenitors (**Figure 1B**). Finally, PCSK9 protein secretion in the cell culture medium measured by ELISA assay paralleled the PCSK9 mRNA and protein variations (**Figure 1C**). Notably, the level of secreted PCSK9 was much higher in hiPSCs than in HLCs. Altogether these data demonstrate that undifferentiated hiPSCs express and secrete PCSK9 at significant level.

PCSK9 inhibition modulates the NODAL signaling pathway and cell proliferation in hiPSCs

In order to investigate the functional role of PCSK9 in this newly described environment, we silenced PCSK9 in hiPSCs using specific shRNA (originally from K3 hiPS cell line - **Supplemental Table 1**) and performed a transcriptomic analysis (DNA-chip Agilent). From the list of differentially expressed genes between iPSCs-shPCSK9 *vs*. iPSCs-shCtrl (**Supplemental Table 2**) we screened for overrepresented biological processes using Gene Ontology (GO) terms in genes downregulated together with PCSK9 in iPSCs-shPCSK9 *vs*. iPSCs-shCtrl. Significant GO biological processes are mainly related to metabolic, biosynthetic and developmental processes (**Supplemental Table 3**). More specifically, the top differentially expressed genes include *PCSK9* itself, with more than 90% inhibition, *NODAL* and NODAL downstream pathway gene target such as *LEFTY2*. RT-Q-PCR analysis further confirmed that *PCSK9*, *NODAL* and *LEFTY1* were significantly down-regulated in PCSK9 silenced hiPSCs (**Figure 2A**). Despite a trend, PCSK9 silencing did not significantly alter *LDLR* mRNA levels (**Figure 2A**). In addition, two other targets of the NODAL signaling pathway, *OCT4* and *NANOG* showed a decreased gene expression. While both OCT3 and NANOG are pluripotent transcription factors expressed also in the mesendoderm, we

monitored the expression of a third pluripotent transcription factor subsequently expressed during ectoderm differentiation, *SOX2*, which was not affected by PCSK9 silencing. In accordance with a functional effect of NODAL pathway gene expression regulation, we observed that the modulation of PCSK9 gene expression affects hiPSCs proliferation. Indeed, the cellular growth curve was significantly reduced in hiPSCs silenced for PCSK9 compared to hiPSCs control (**Figure 2B**).

To further study the impact of PCSK9 on the NODAL signaling pathway in undifferentiated cells, we generated two cellular models that were studied side by side. We first generated a PCSK9 knock-out (KO) hiPSCs (PCSK9-KO) with a CRISPR/Cas9 system (from hERG control cell line- Supplemental **Table 1**). We also generated a stable hiPS cell-line overexpressing PCSK9 (PCSK9-FULL) through the integration of PCSK9 at the AAVS1 locus (from hERG control cell line). Western blot analysis confirmed that PCSK9 protein expression was totally lost in PCSK9-KO hiPSCs and strongly increased in PCSK9-FULL hiPSCs (**Figure 3A**). Then, we assessed the cell proliferation of PCSK9-KO and PCSK9-FULL hiPSCs (**Figure 3B**). In line with the previous results, while PCSK9-KO hiPSCs present a significantly reduced cell growth, the proliferation of PCSK9-FULL hiPSCs was significantly increased. Next, we investigated the phosphorylation state of the NODAL signaling pathway mediator, SMAD2. A shown in **Figure 3C,** SMAD2 phosphorylation status was reduced in PCSK9-KO hiPSCs, while it was increased in PCSK9-FULL hiPSCs, further validating the hypothesis of an impact of PCSK9 on the NODAL signaling pathway.

In order to further strengthen our previous observations and validate them in patients' material with non-genetically engineered hiPSCs, we generated and studied hiPSCs of a patient carrying the PCSK9 LOF mutations R104C/V114A. This patient presented with genetically low levels of LDL-C (*i.e.* familial hypobetalipoproteinemia) and an absence of liver-derived circulating PCSK9 (Cariou et al., 2009). Previous *in vitro* investigations suggested that R104C/V114A mutations prevented PCSK9 auto-cleavage, its subsequent secretion and acted as a dominant negative mutant (Cariou et al., 2009). Indeed, we observed that PCSK9 auto-cleavage was drastically diminished in R104C/V114A hiPSCs, resulting in a higher proportion of uncleaved non-mature form of PCSK9 (**Figure 4A**). In accordance with PCSK9-KO hiPSCs results, the cellular growth and the phosphorylated form of SMAD2, were decreased in hiPSCs R104C/V114A compared to the control hiPSCs (**Figure 4B and C**). Finally, we monitored the effect of the R104C/V114A LOF mutations on the overall TGFß signaling pathway upon the introduction of a TGFß-gene reporter through luciferase activity in the control and patient-derived hiPSC lines (Huang et al., 2011). As depicted in

Figure 4D, PCSK9 R104C/V114A hiPSCs present with a drastic reduction of the luciferase activity when compared to controls.

Altogether, our data indicate that PCSK9 inhibition, due to either CRISPR-mediated knockout or LOF mutations, decreases the NODAL signaling pathway.

PCSK9 deficiency decreases TGFβR1 content in hiPSCs potentially trough an up-regulation of DACT2

To further precise the mechanism of action of PCSK9 on the NODAL signaling pathway, we added the recombinant wild-type PCSK9 (rPCSK9-WT) or an overactive recombinant form of PCSK9 (rPCSK9-D374Y) in control hiPSCs culture medium over 24h. The addition of rPCSK9-WT or rPCSK9-D374Y in the medium did not affect the SMAD2 phosphorylation status (**Supplemental Figure 1**), suggesting that PCSK9 interferes with the NODAL pathway intracellularly rather than extracellularly.

Then, we tried to overcome the downregulation of NODAL signaling associated to PCSK9 deficiency by adding recombinant NODAL protein (up to 200 ng/mL during 2 hours) in the culture medium of either control or PCSK9 R104C/V114A hiPSCs. In contrast to what was observed in control hiPSCs, NODAL was unable to induce SMAD2 phosphorylation in R104C/V114A hiPSCs (**Supplemental Figure 2**), suggesting that PCSK9 is required for NODAL activity in hiPSCs.

Based on these results, we hypothesized that PCSK9 might directly interfere with NODAL signaling at the TGFß receptor subunit 1 (TGFßR1) level. We measured the abundance of TGFßR1 at the cell surface in different hiPSC lines using a biotinylation assay. While the TGFßR1 content was consistently lowered in both PCSK9-KO and R104C/V114A hiPSCs compared to control hiPSCs, no significant difference was detected in PCSK9-FULL hiPSCs (**Figure 5**).

TGFßR1 has been described as a target of the Disheveld Antagonist of ß-Catenin 2 (DACT2), which is located in late endosomes and induces TGFßR1 lysosomal degradation (Zhang et al., 2004). Through western blot analysis, we found that the expression of DACT2 (isoform: ENSP00000476434, Q5SW24; 40 kDa) was significantly increased in PCSK9-KO hiPSCs as well as in R104C/V114A hiPSCs when compared to controls (**Figure 6A & B**). In contrast, we did not observe changes in DACT2 protein expression in PCSK9-FULL hiPSCs **(Figure 6C)**. In order to verify whether PCSK9 could interact intracellularly with DACT2 in hiPSCs we generated several hiPSC lines expressing either: i) the V5-tagged-PCSK9-full-protein (FL-PCSK9 hiPSCs), ii) the V5-tagged-PCSK9-protein lacking the prodomain and

catalytic domain (CHRD hiPSCs) or iii) the V5-tagged-PCSK9-protein lacking (L455X hiPSCs) (**Figure 7A**). Upon V5-mediated PCSK9 pull-down, we found that the DACT2 40kDa isoform was co-immunoprecipitated with V5-PCSK9 in FL-PCSK9 hiPSCs (**Figure 7B**). Moreover, while DACT2 was also detected in CHRD hiPSCs, it was lost with the L455X-construct, suggesting that PCSK9 interacts with DACT2 *via* its CHRD domain.

Taken together, these data suggest that intra-cellular PCSK9 may modulate TGFßR1 signaling pathway by regulating DACT2 expression.

DISCUSSION

In the present study, we report for the first time that PCSK9 is expressed at a high level in hiPSCs. While PCSK9 expression is maximal in the undifferentiated state, it decreases during the hepatic differentiation program before a final rebound in the late HLCs differentiation steps. From a functional point of view, we showed that PCSK9 controls the cellular proliferation of hiPSCs. Regarding the molecular mechanisms, we demonstrated that PCSK9 interferes with the NODAL/SMAD2 signaling pathway at least by interacting with DACT2, an inhibitor of TGFßR1. In our working model, PCSK9 leads to a degradation of DACT2, thereby stimulating the NODAL pathway and the cellular proliferation of hiPSCs.

Importantly, our work opens novel perspectives in the field of PCSK9 biology by identifying: i) a novel cellular environment for PCSK9 action, which is not restricted to mature hepatocytes; ii) a novel function for PCSK9 - the regulation of hiPSCs proliferation which is independent of the LDLR pathway; and iii) a potential novel PCSK9 binding partner – DACT2.

While PCSK9 is mainly expressed in mature hepatocytes, it is expressed in many tissues and cells (Cariou et al., 2015; Seidah et al., 2003). It should be reminded here that PCSK9 was initially cloned in primary cerebellar neurons under apoptotic stimulus (Seidah et al., 2003). In order to gain insights on the potential new functions of PCSK9 in hiPSCs, we performed unbiased transcriptomic approaches after manipulating PCSK9 gene expression. Interestingly, the NODAL pathway (*i.e* NODAL itself and its target genes such as LEFTY1 and 2) appears significantly downregulated by silencing of PCSK9. We further confirmed that manipulating PCSK9 expression consistently affects SMAD2 phosphorylation status, that we used as a readout of the NODAL signaling pathway. Of functional relevance, we demonstrated by using complementary models (PCSK9 KO and PCSK9 R104C/V114A LOF mutant) that PCSK9 deficiency in hiPSCs is associated with a reduced cell proliferation. Conversely, PCSK9 overexpression in hiPSCs led to both increased NODAL signaling and cell proliferation.

From a mechanistic point of view, we first assessed whether PCSK9 interfere with NODAL signaling in an intra-cellular or extra-cellular manner. Our data indicate that 24 hours exposure to extracellular recombinant PCSK9 has no effect on SMAD2 phosphorylation, suggesting that PCSK9 may act on TGFßR1 and its downstream signaling pathway mostly through an intracellular effect. In addition, we showed that the addition of

recombinant NODAL did not restore SMAD2 phosphorylation in PCSK9-deficient hiPSCs. Although we cannot exclude the hypothesis that PCSK9 is necessary for the signaling action of NODAL *per se,* our data suggest that PCSK9 instead interfere with the abundance of TGFßR1 at the cell surface. The decreased TGFßR1 expression observed in the context of PCSK9 deficiency could explain the reduced NODAL signaling and its resistance to recombinant NODAL treatment.

Therefore, we sought for intracellular regulator of TGFBR1. The disheveled antagonist of ß-catenin (DACT) family has been described as scaffold proteins involved in cell signaling regulation (Cheyette et al., 2002; Su et al., 2007; Zhang et al., 2004). While DACT1 mostly regulate the Wnt signaling pathways through disheveled lysosomal degradation (Cheyette et al., 2002; Su et al., 2007; Zhang et al., 2004), DACT2 has been described as an inhibitor of the NODAL receptor in zebrafish (Zhang et al., 2004) by binding and targeting it to lysosomal degradation. Su et *al.* have verified this mechanism in mammalian cells (Su et al., 2007).

Based on these observations, we considered DACT2 as a potential target of PCSK9 and studied its content at the protein level in our different hiPS cell lines. Importantly, we confirmed that the silencing or inhibition of PCSK9 is associated with an increased DACT2 protein content, which is in line with the reduced TGFBR1 expression at the plasma membrane. Although PCSK9 overexpression induced SMAD2 phosphorylation and in a lesser extent cell proliferation, we failed to detect a significant decrease in DACT2 and subsequent increase in TGFßR1 expression. The reason for this discrepancy remains unclear but can be due to non-physiological stochiometric changes related to massive PCSK9 overexpression.

Finally, to highlight the potential interaction between PCSK9 and DACT2 we conducted several co-immunoprecipitation experiments and were able to co-immunoprecipitate PCSK9 and DACT2 in undifferentiated hiPSCs. Using truncated forms of PCSK9 stably overexpressed in hiPSCs, we showed that the Cys-His-rich domain (CHRD) was mainly involved in this interaction. The same domain is involved in the interaction between PCSK9 and the LDLR before their trafficking to the lysosomal pathway (Nassoury et al., 2007). In the light of our results, additional experiments remain to be conducted in order to establish whether this interaction is direct or indirect.

Our findings open new interesting perspectives for PCSK9 biology in at least two fields of research: development and cancer.

NODAL is involved in embryonic stem (ES) cells pluripotency maintenance in mouse and human (Vallier et al., 2009) and crucial for their differentiation (Chng et al., 2010). It is therefore conceivable that PCSK9 contributes to pluripotent stem cell regulatory mechanisms by stimulating the NODAL pathway. Of note, the NODAL function on ES cells seems to be species-specific, with no similar effect in mouse compared to human ES cells (James et al., 2005). This observation can be related to the absence of developmental effect of *Pcsk9* deficiency in mice (Rashid et al., 2005). In contrast, there are several arguments for a potential role for PCSK9 in human development. Firstly, it is intriguing that only very few patients were described with LOF mutations in both alleles of *PCSK9* and virtually none with a complete PCSK9 deficiency have been identified world-wide (Cariou et al., 2009; Zhao et al., 2006). Secondly, PCSK9 has been suggested to be potentially involved in the pathogenesis of neural tube defects (NTDs), due to an association between maternal plasma PCSK9 levels and fetal NTDs risk (An et al., 2015). This observation is reinforced by the findings that NODAL and DACT2 have been shown to be involved in the control of neurulation (Gonsar et al., 2016) and the delamination of neural crest cells (Rabadán et al., 2016) respectively.

Although the NODAL pathway is almost not operational after the period of embryonic development, several studies have highlighted an upregulation of NODAL activity in many human cancers. For instance, increased expression of NODAL has been shown to be correlated with disease progression in malignant melanoma (Topczewska et al., 2006). It is intriguing to note that PCSK9 deficiency reduces melanoma metastasis in mouse livers (Sun et al., 2012). While one mechanistic hypothesis for the link between PCSK9 and cancer progression is the modulation of cholesterol supply to the tumor (Huang et al., 2016), a recent paper described PCSK9 as a regulator of the major histocompatibility protein class I (MHCI) recycling by promoting its relocation and degradation in the lysosome (Liu et al., 2020). This result identified PCSK9 as a promising strategy in cancer immunotherapy (Almeida et al., 2021). Our data suggest that PCSK9 may directly regulates cell proliferation, potentially through a modulation of NODAL signaling. Thus, it would be interesting to assess whether PCSK9 can also regulate NODAL pathway and cell proliferation in the context of cancer.

Our study has several limitations that should be highlighted. As discussed earlier, the PCSK9 overexpression model does not perfectly mirror the abnormalities observed in the PCSK9 deficiency models, notably regarding the regulation of DACT2 and TGFBR1. Direct evidence that PCSK9 regulates cell proliferation exclusively in a NODAL-dependent manner

is missing. The co-immunoprecipitation experiments with DACT2 were performed with overexpressed PCSK9-V5 constructs and not with endogenous PCSK9. Finally, some hiPSCs lines carry a CNV in the 20th chromosome. Noticeably, all the target genes analyzed in the present study are not located in this genomic area, especially those of the NODAL signaling pathway.

In conclusion, our study highlights a new function for PCSK9 in hiPSCs proliferation potentially through the modulation of the NODAL signaling pathway. These findings open up new perspectives on the potential link between PCSK9 and embryonic development and/or cancer progression or development. Since there are currently some reflections about the potency of therapeutic PCSK9 inhibition using genomic editing approaches (Musunuru et al., 2021), it is critical to have a clear understanding of PCSK9 biology to avoid potential long-term side effects.

EXPERIMENTAL PROCEDURES

Ethic statement

The study was conducted in compliance with current Good Clinical Practice standards and in accordance with the principles set forth under the Declaration of Helsinki (1989). Each subject entering the study agreed to and signed an institutional review board-approved statement of informed consent for the collection of urine samples (authorization number from the French Ministry of Health: DC-2011-1399).

Human iPSCs culture and differentiation

hiPSCs culture.

Reprogramming and characterization of the hiPSC lines were described in previous publications (Si-Tayeb et al., 2010, 2016), see **Supplemental Table 1** for further information on cell lines. HiPSCs were cultured on plates coated with Matrigel (Corning; 0.05 mg/ml) in StemMACS iPS-Brew medium (Miltenyi) and passages were performed using the Gentle Cell Dissociation Buffer (Stem Cell Technologies). Genomic integrity of hiPSC lines was tested using digital PCR of copy number variants (CNVs) of the main human recurrent genomic abnormalities (Stemgenomics, Montpellier, France), see **supplemental Table 1** and supplemental data for CNVs reports. Briefly, all cell lines tested had a good quality control with no CNVs measured except for the PCSK9-FULL overexpression cell line and both K3 sh-control and sh-PCSK9 which carry a gain in the 20^{th} chromosome.

hiPSCs differentiation into HLCs

hiPSCs-control were differentiated into HLCs as previously described (Si-Tayeb et al., 2016) in triplicates. Briefly, once cells reach ~70-80% confluency, hiPSCs were cultured in RPMI 1640 medium (Life Technologies) supplemented with B27 (with insulin) (Life Technologies), Activin A 100 ng/ml (Miltenyi), FGF2 20 ng/ml (Miltenyi) and BMP4 10 ng/ml (Miltenyi) for 2 days in normoxia (20% O2, 5% CO2), then switched to RPMI 1640 with Activin A 100 ng/ml for three days to induce definitive endoderm cells (DE). DE cells were further differentiated into hepatic progenitor cells for 5 days in RPMI supplemented with BMP4 20 ng/ml and FGF2 10 ng/ml in hypoxia (4% O2, 5% CO2). Then cells were cultured for 5 days into immature hepatocytes in RPMI 1640 supplemented with HGF 20 ng/ml (Miltenyi) in hypoxia (4% O2, 5% CO2). Then, cells were directed into mature hepatocytes being cultured in hepatocyte culture medium (HCM) (Lonza) supplemented with Oncostatin M 20 ng/ml (Miltenyi) for additional 5-6 days in normoxia (20% O2, 5% CO2). RNA samples were collected at every day of the differentiation (day 0 to day 20) and processed further for Quantitative Polymerase Chain Reaction (qPCR) (detailed explanation is shown in the gene

expression analysis). 24h conditioned medium was collected, centrifuged then kept for further secretion study using an ELISA assay kit.

Recombinant proteins and chemical treatments

Undifferentiated hiPSCs were treated for 2 hours with recombinant Nodal (R&D, 3218-ND-025) at concentrations ranging from 10 to 200ng/mL in StemMACS iPS-Brew medium without supplements (Miltenyi).

Undifferentiated hiPSCs were treated for 24 hours with the wild type PCSK9 recombinant protein (rPCSK9-WT; Circulex, CY-R2330) or the gain of function D374Y-PCSK9 recombinant protein (rPCSK9 D374Y (Circulex, CY-R2311) at concentration of 600ng/mL in the routinely used hiPSC culture medium, for each recombinant protein.

Transcriptomic analysis

RNA samples were prepared and hybridized on Agilent Human Gene Expression 8×60 K microarrays (Agilent Technologies, part number: G4851A). Normalization procedures were performed using R statistical software (http://www.r-project.org). The raw signals of all probes for all the arrays were normalized against a virtual median array (median raw intensity per row) using a local weighted scattered plot smoother analysis (LOWESS). The data were filtered to remove probes with low intensity values. This filtering is performed by sample category in order to keep the signature of categories with a small sample size. A hierarchical clustering was computed on median-gene-centered and log-transformed data using average linkage and uncentered correlation distances with the Cluster program. We ran a Gene Ontology analysis on differentially expressed genes in order to identify biological processes overrepresented using the PANTHER Overrepresentation test (PANTHER version 16.0 - Released 20210224) (Mi et al., 2021).

Gene expression analysis

RNA samples were isolated using the RNeasy Mini Kit (Qiagen). Reverse transcription of 1µg of RNA into cDNA was conducted using the high-capacity cDNA reverse-transcription kit (Applied Biosystems). Conditions were as follows: 10 min at 25°C, and then 2 hours at 37°C. Quantitative Polymerase Chain Reaction (qPCR) studies were conducted in triplicate using the brilliant III Ultra-Fast Master Mix with high ROX (Agilent). Primers sequences are listed in ***supplemental Table 4***. Each qPCR included 2 s at 50°C, 10 s at 95°C followed by 40 cycles of 15 s at 95°C, and 60 s at 60°C. Cycle threshold was calculated by using default settings for the real time sequence detection software (Applied Biosystems).

Protein expression analysis

hiPSCs were lysed in modified RIPA buffer composed of 150 mM NaCl, 50 mM Tris HCl pH 8, 1% NP-40 (Nonidet P-40) and 0,1% SDS at pH 7.4 and containing a cocktail of protease inhibitors (Sigma Aldrich) and phosphatase inhibitors (Sigma Aldrich). Total cell lysates were then passed 10 times through a fine gauge needle followed by sonication (5 pulses for 5 sec each). A protein assay was then carried out against a range of standard bovine serum albumin (BSA) using PierceTM BCA Protein Assay Kit. The lysates were denatured for 10 min at 70 °C in a mixture of NuPAGE® Sample Reducing Agent (10X) that contains dithiothreitol (DTT) (500 mM) and NuPAGE® LDS Sample Buffer (4X) containing 2% LDS (lithium dodecyl sulfate), 10% glycerol, 141 mM Tris Base, 106 mM Tris HCl, 0.51 mM EDTA, 0.51 mM EDTA, 0.175 mM Phenol Red and pH 8.5. 25 micrograms of each sample were loaded onto a 10% polyacrylamide gel or onto a Bis-Tris NuPAGE™ Novex™ 4 to 12 % (Invitrogen) and the proteins were separated by electrophoresis in presence of SDS. After migration, the proteins are transferred to nitrocellulose membrane (Bio-Rad) using Trans-Blot Turbo Transfer System (Bio-Rad). Revelation and quantification were done by Image Lab software (Bio-Rad). The membrane was saturated for one hour in TBS-T buffer (10 mM Tris, NaCl 0.5 mM and 0.1% Tween-20) containing 5% skimmed milk lyophilized. The membrane was then incubated with primary antibody overnight at 4°C in TBS-T milk. Horseradish peroxidase (HRP)-conjugated secondary antibody staining was performed for 1 h at room temperature (RT) in TBS-T milk. Protein bands were detected using ECL detection system (Bio-Rad) and ECL Clarity max (Ref) when required. Antibody references and dilutions are listed in **supplemental Table 5.**

PCSK9 ELISA assay

PCSK9 levels in conditioned medium were assayed in duplicates using a commercially available quantitative sandwich ELISA assay following the manufacturer's instructions (Circulex CY-8079, CycLex Co.).

PCSK9 silencing in hiPSCs

PCSK9 gene expression has been silenced upon lentiviral transduction of specific shRNA (Sigma). The clone TRCN0000075236 cloned into the pLKO.1-Puro vector has been used to target PCSK9 while an unspecific shRNA sequence has been used as control. Upon transduction, K3 hiPSCs (Si-Tayeb et al., 2010) were subjected to Puromycin (TOCRIS Bioscience 4089/50) selection using a concentration up to 8µg/ml.

PCSK9 knockout in control hiPS cells was generated using the Alt-R™ CRISPR-Cas9 System (Integrated DNA Technologies) targeting the exon 7 of PCSK9 at both alleles. Briefly gRNA CCAGCGACTGCAGCACCTGC was first duplexed with the Alt-R® CRISPR-Cas9

tracrRNA, then complexed to the Alt-R® S.p. Cas9 Nuclease according to IDT recommandations. The complex was delivered into control hiPSCs previously generated (Si-Tayeb et al., 2016) using Amaxa nucleofection (Lonza) and hiPSCs were cultured on mouse embryonic fibroblasts (MEFs) in hiPSCs medium composed of DMEM/F12 (Life Technologies) supplemented with 20% Knockout Serum Replacer (Life Technologies), 0.5% L-Glutamine (Life Technologies) with 0.14% β-mercaptoethanol (Sigma), 1% NEAA and 5 ng/ml fibroblast growth factor 2 (FGF2, Miltenyi) in hypoxia (4% O2, 5% CO2). Colonies were manually picked from MEFs for cloning strategy then cultured in 96 wells plates under feeder free culture conditions as described earlier. Genotyping of engineered nuclease-induced mutations was performed using T7 endonuclease assay (NEB) followed by PCR sequencing.

Plasmid constructs and hiPS cell lines selection

The TGF-β sensitive promoter upstream the luciferase coding sequence or the sequence coding for FL-PCSK9, L455X and CHRD were inserted in the AAVS1 site located in chromosome 19 of hiPSCs control and in hiPSCs carrying the *PCSK9* R104C/V114A LOF variant for the luciferase construct only. Briefly, the luciferase construct has been removed from the 3TP-lux plasmid (Addgene #11767) while sequence of FL-PCSK9, L455X and CHRD were removed from the p-IRES2-EGFP plasmids kindly given by Prof Nabil Seidah's laboratory (Nassoury et al., 2007). Removed sequences were sub-cloned in the AAVS1-hPGKPuro-PA donor (Addgene #22072). Specific AAVS1 insertion has been performed upon nucleofection (Amaxa, Lonza) of the new construct together with plasmids encoding for hAAVS1 1R TALEN (Addgene #35432) and hAAVS1 1L TALEN (Addgene #35431) homologous sequences as previously described (Hockemeyer et al., 2011). Thereafter, hiPSCs were selected with Puromycin (TOCRIS Bioscience 4089/50; up to 8µg/ml) and correct construction insertion has been verified by PCR sequencing

Co-Immunoprecipitation of V5-PCSK9 constructs

The co-Immunoprecipitation (co-IP) was carried out using the magnetic Dynabeads® Protein G immunoprecipitation kit (Life technologies). 50 µl of Dynabeads were conjugated with 2 µg of V5 antibody (sc-81594) or IgG control (sc-3877) and incubated at RT for 10 min with rotation. The beads were washed three times in 200 µl lysis buffer and then incubated with 500 µg of total lysates at +4 °C for 2 hours with rotation. Supernatant was then discarded and the beads were washed three times in 200 µl lysis buffer + Tween 0.05% at +4 °C. Beads-protein complexes are then heated for 10 min at 70 °C in 30 µl of a mixture of the NuPAGE® Sample Reducing Agent (10X) and LDS Sample Buffer (4X). The samples were placed on

the magnet and the attached protein/protein complexes were collected and loaded onto a Bis-Tris NuPAGE™ Novex™ 4 to 12 % (Invitrogen). 25 µg of protein were used as an input.

Biotinylation assay

Cells were washed 2 times with 2 mL ice-cold 1X PBS with calcium and magnesium (Sigma-Aldrich, D8662). Cells were incubated with 1 ml previously dissolve Sulfo-NHS-SS-biotin (Pierce, #21331) in iPS Brew Media (Miltenyi, 130-104-368) to final concentration 0.5mg/ml and agitate 30 min in ice. Biotin solution was discarded and cells were washed 4 times with 2 ml Tris-saline solution (10mM Tris-HCl, pH 7.5, 120mM NaCl). 150 µl of lysis buffer were added on cells, scrape, triturate, rotate for 15 min at 4°C and centrifuge 3000 rpm for 10 min at +4°C. Biotinylated proteins were added (1mg) to 100µl Immobilized NeutrAvidin beads (Pierce, #29200) previously wash 2 times with lysis buffer. Incubate with rotation for 2 hours at +4°C. Beads were washed 3 times with 1ml lysis buffer (centrifugation 2500 rpm for 30sec) and were eluted with 70 µl 1X SDS sample buffer (Invitrogen, NP0007) + 100 mM DTT at 50°C for 30 min.

Luciferase assay

Basal luciferase activity was detected with the Luciferase Assay System (Promega) by following the manufacturer's instructions. Briefly, 106 cells were plated per well of a 6-well-plate, and cultured overnight at 37°C, 5% CO2, 4% O2. Cells were then washed twice and incubated with a specific lysis buffer before freezed at -20 °C for 30 min. Once thawed, the cell lysate was centrifuged and the luciferase assay was performed on the supernatant. Luminescence at 10sec was measured using Perkin Elmer VICTOR™ X3 Multilabel Plate Reader.

Proliferation assay

MTT (3-(4,5-dimethylthiazol-2-yl)-2,5-diphenyltetrazolium bromide) tetrazolium assay was used to assess the proliferation of hiPSCs. Briefly, hiPSCs were plated onto 96-well-plates previously coated with Matrigel 0.05 mg/ml in quintuplicates at 2,500 cells/well with ROCK inhibitor (0.01M, CellGuidance). The day after the passage and the third day, media was changed and supplemented with puromycin for the shRNA-expressing cells (TOCRIS Bioscience, 8 µg/ml). Cells were then incubated for 3h at 37°C with MTT solution (Sigma Aldrich M5655) at 0,8mg/mL in culture medium. The resulting purple-colored formazan crystals were then solubilized using DMSO. Finally, the absorbance was read at 540 nm using Perkin Elmer VICTOR™ X3 Multilabel Plate Reader or VARIOSKAN LUX (Thermoscientific). The proliferation rate was monitored over 24hrs, 48h, 72h and 96h.

Statistical analysis

Data are expressed as mean ±s.e.m. Significant differences between mean values were determined with the Mann–Whitney U-test for comparison of two groups or paired Student's t-test if appropriate. For the cluster approach, genes belonging to the same biological function or cell type are known to exhibit correlated expression. We use hierarchical clustering to detect groups of correlated genes supported by a statistical method (limma) to detect differential expression among biological conditions.

DATA AND CODE AVAILABILITY

Metadata, raw and normalized data have been deposited in the Gene Expression Omnibus database (GSE181610, https://www.ncbi.nlm.nih.gov/geo/query/acc.cgi?acc=GSE181610).

ACKNOWLEDGMENTS

This study was supported by a grant from the Fondation Leducq (#13CVD03); the foundation GENAVIE; and the French national research project CHOPIN (CHolesterol Personalized INnovation) funded by the Agence Nationale de la Recherche (ANR-16-RHUS-0007) and coordinated by the CHU of Nantes., the VaCaRMe project funded by the Région Pays de la Loire, the CHU of Nantes, the Lebanese University President grant and a CIFRE grant funded by HCS Pharma.

We are most grateful to the Bioinformatics Core Facility of Nantes BiRD, member of Biogenouest, Institut Français de Bioinformatique (IFB) (ANR-11-INBS-0013) for the use of its resources and for its technical support. AR is supported by post-doctoral fellowship grants from the “Fondation Recherche Médicale” and from the “Institut de France-Fondation Lefoulon-Delalande”.

AUTHOR CONTRIBUTIONS

M.R., S.I., A.C., B.C., and K.S-T. designed the experiments. M.R., S.I., A.C., A.G., B.C., A.D., A.L., L.A., M.P., A.P. and N.G.S. performed the experiments. M.R., S.I, A.C., A.G, A.R, B.C., K.S-T. analyzed the data. M.R., S.I., A.C, A.G, C.L-M., K.Z., B.C. and K.S-T wrote the paper. A.R., X.P. C.L-M. contributed to the discussion. B.C. supported the work of M.R., A.C., A.G., B.C., A.D., A.L. and K.S-T. K.Z., supported the work of S.I. K.S-T conceived the project.

DECLARATION OF INTERESTS

B.C. has received research funding from Amgen, Pfizer and Sanofi and Regeneron Pharmaceuticals Inc outside of the present work; and has served on scientific advisory boards and received honoraria or consulting fees from Amgen, Regeneron and Sanofi. The other authors declare no conflict of interest.

REFERENCES

Abifadel, M., Varret, M., Rabès, J.P., Allard, D., Ouguerram, K., Devillers, M., Cruaud, C., Benjannet, S., Wickham, L., Erlichje vais 4–156.

Almeida, C.R., Ferreira, B.H., and Duarte, I.F. (2021). Targeting PCSK9: a promising adjuvant strategy in cancer immunotherapy. Sig Transduct Target Ther *6*, 111.

An, D., Wei, X., Li, H., Gu, H., Huang, T., Zhao, G., Liu, B., Wang, W., Chen, L., Ma, W., et al. (2015). Identification of PCSK9 as a novel serum biomarker for the prenatal diagnosis of neural tube defects using iTRAQ quantitative proteomics. Scientific Reports *5*, 17559.

Assou, S., Le Carrour, T., Tondeur, S., Ström, S., Gabelle, A., Marty, S., Nadal, L., Pantesco, V., Réme, T., Hugnot, J.-P., et al. (2007). A meta-analysis of human embryonic stem cells transcriptome integrated into a web-based expression atlas. Stem Cells *25*, 961–973.

Benjannet, S., Rhainds, D., Essalmani, R., Mayne, J., Wickham, L., Jin, W., Asselin, M.-C., Hamelin, J., Varret, M., Allard, D., et al. (2004). NARC-1/PCSK9 and its natural mutants: zymogen cleavage and effects on the low density lipoprotein (LDL) receptor and LDL cholesterol. The Journal of Biological Chemistry *279*, 48865–48875.

Calloni, R., Cordero, E.A.A., Henriques, J.A.P., and Bonatto, D. (2013). Reviewing and updating the major molecular markers for stem cells. Stem Cells Dev *22*, 1455–1476.

Cariou, B., Ouguerram, K., Zaïr, Y., Guerois, R., Langhi, C., Kourimate, S., Benoit, I., Le May, C., Gayet, C., Belabbas, K., et al. (2009). PCSK9 dominant negative mutant results in increased LDL catabolic rate and familial hypobetalipoproteinemia. Arteriosclerosis, Thrombosis, and Vascular Biology *29*, 2191–2197.

Cariou, B., Si-Tayeba, K., and Le Maya, C. (2015). Role of PCSK9 beyond liver involvement. Current Opinion in Pediatrics *26*, 155–161.

Catapano, A.L., Pirillo, A., and Norata, G.D. (2020). New Pharmacological Approaches to Target PCSK9. Current Atherosclerosis Reports *22*.

Cheyette, B.N.R., Waxman, J.S., Miller, J.R., Takemaru, K.I., Sheldahl, L.C., Khlebtsova, N., Fox, E.P., Earnest, T., and Moon, R.T. (2002). Dapper, a Dishevelled-associated antagonist of β-catenin and JNK signaling, is required for notochord formation. Developmental Cell *2*, 449–461.

Chng, Z., Teo, A., Pedersen, R.A., and Vallier, L. (2010). SIP1 Mediates Cell-Fate Decisions between Neuroectoderm and Mesendoderm in Human Pluripotent Stem Cells. Cell Stem Cell *6*, 59–70.

Cohen, J.C., Boerwinkle, E., Mosley, T.H., and Hobbs, H.H. (2006). Sequence variations in PCSK9, low LDL, and protection against coronary heart disease. New England Journal of Medicine *354*, 1264–1272.

Ference, B.A., Robinson, J.G., Brook, R.D., Catapano, A.L., Chapman, M.J., Neff, D.R., Voros, S., Giugliano, R.P., Davey Smith, G., Fazio, S., et al. (2016). Variation in *PCSK9* and *HMGCR* and Risk of Cardiovascular Disease and Diabetes. New England Journal of Medicine *375*, 2144–2153.

Gonsar, N., Coughlin, A., Clay-Wright, J.A., Borg, B.R., Kindt, L.M., and Liang, J.O. (2016). Temporal and spatial requirements for Nodal-induced anterior mesendoderm and mesoderm in anterior neurulation. Genesis *54*, 3–18.

Hockemeyer, D., Wang, H., Kiani, S., Lai, C.S., Gao, Q., Cassady, J.P., Cost, G.J., Zhang, L., Santiago, Y., Miller, J.C., et al. (2011). Genetic engineering of human pluripotent cells using TALE nucleases. Nat Biotechnol *29*, 731–734.

Huang, J., Li, L., Lian, J., Schauer, S., Vesely, P.W., Kratky, D., Hoefler, G., and Lehner, R. (2016). Tumor-Induced Hyperlipidemia Contributes to Tumor Growth. Cell Reports *15*, 336–348.

Huang, T., David, L., Mendoza, V., Yang, Y., Villarreal, M., De, K., Sun, L., Fang, X., López-Casillas, F., Wrana, J.L., et al. (2011). TGF-β signalling is mediated by two

autonomously functioning TβRI:TβRII pairs. EMBO Journal *30*, 1263–1276.
James, D., Levine, A.J., Besser, D., and Hemmati-Brivanlou, A. (2005). TGFbeta/activin/nodal signaling is necessary for the maintenance of pluripotency in human embryonic stem cells. Development *132*, 1273–1282.
Liu, X., Bao, X., Hu, M., Chang, H., Jiao, M., Cheng, J., Xie, L., Huang, Q., Li, F., and Li, C.-Y. (2020). Inhibition of PCSK9 potentiates immune checkpoint therapy for cancer. Nature *588*, 693–698.
Maxwell, K.N., and Breslow, J.L. (2004). Adenoviral-mediated expression of Pcsk9 in mice results in a low-density lipoprotein receptor knockout phenotype. Proceedings of the National Academy of Sciences of the United States of America *101*, 7100–7105.
Mi, H., Ebert, D., Muruganujan, A., Mills, C., Albou, L.-P., Mushayamaha, T., and Thomas, P.D. (2021). PANTHER version 16: a revised family classification, tree-based classification tool, enhancer regions and extensive API. Nucleic Acids Research *49*, D394–D403.
Musunuru, K., Chadwick, A.C., Mizoguchi, T., Garcia, S.P., DeNizio, J.E., Reiss, C.W., Wang, K., Iyer, S., Dutta, C., Clendaniel, V., et al. (2021). In vivo CRISPR base editing of PCSK9 durably lowers cholesterol in primates. Nature *593*, 429–434.
Nassoury, N., Blasiole, D.A., Tebon Oler, A., Benjannet, S., Hamelin, J., Poupon, V., McPherson, P.S., Attie, A.D., Prat, A., and Seidah, N.G. (2007). The Cellular Trafficking of the Secretory Proprotein Convertase PCSK9 and Its Dependence on the LDLR. Traffic *8*, 718–732.
Pauklin, S., and Vallier, L. (2015). Activin/Nodal signalling in stem cells. Development *142*, 607–619.
Poirier, S., Mayer, G., Poupon, V., McPherson, P.S., Desjardins, R., Ly, K., Asselin, M.C., Dy, R., Duclos, F.J., Witmer, M., et al. (2009). Dissection of the endogenous cellular pathways of PCSK9-induced low density Lipoprotein receptor degradation. Evidence for an intracellular route. Journal of Biological Chemistry *284*, 28856–28864.
Preiss, D., Tobert, J.A., Hovingh, G.K., and Reith, C. (2020). Lipid-Modifying Agents, From Statins to PCSK9 Inhibitors: JACC Focus Seminar. Journal of the American College of Cardiology *75*, 1945–1955.
Rabadán, M.A., Herrera, A., Fanlo, L., Usieto, S., Carmona-Fontaine, C., Barriga, E.H., Mayor, R., Pons, S., and Martí, E. (2016). Delamination of neural crest cells requires transient and reversible Wnt inhibition mediated by Dact1/2. Development (Cambridge) *143*, 2194–2205.
Rashid, S., Curtis, D.E., Garuti, R., Anderson, N.H., Bashmakov, Y., Ho, Y.K., Hammer, R.E., Moon, Y.A., and Horton, J.D. (2005). Decreased plasma cholesterol and hypersensitivity to statins in mice lacking Pcsk9. Proceedings of the National Academy of Sciences of the United States of America *102*, 5374–5379.
Seidah, N.G., Benjannet, S., Wickham, L., Marcinkiewicz, J., Bélanger Jasmin, S., Stifani, S., Basak, A., Prat, A., Chrétien, M., Jasmin, S.B., et al. (2003). The secretory proprotein convertase neural apoptosis-regulated convertase 1 (NARC-1): Liver regeneration and neuronal differentiation. *100*, 928–933.
Seidah, N.G., Abifadel, M., Prost, S., Boileau, C., and Prat, A. (2017). The proprotein convertases in hypercholesterolemia and cardiovascular diseases: Emphasis on proprotein convertase subtilisin/Kexin 9. Pharmacological Reviews *69*, 33–52.
Si-Tayeb, K., Noto, F.K., Sepac, A., Sedlic, F., Bosnjak, Z.J., Lough, J.W., and Duncan, S.A. (2010). Generation of human induced pluripotent stem cells by simple transient transfection of plasmid DNA encoding reprogramming factors. BMC Developmental Biology *10*, 81.
Si-Tayeb, K., Idriss, S., Champon, B., Caillaud, A., Pichelin, M., Arnaud, L., Lemarchand, P., Le May, C., Zibara, K., and Cariou, B. (2016). Urine-sample-derived human induced pluripotent stem cells as a model to study PCSK9-mediated autosomal dominant

hypercholesterolemia. Disease Models & Mechanisms *9*, 81–90.
Stoekenbroek, R.M., Lambert, G., Cariou, B., and Hovingh, G.K. (2018). Inhibiting PCSK9 - biology beyond LDL control. Nat Rev Endocrinol *15*, 52–62.
Su, Y., Zhang, L., Gao, X., Meng, F., Wen, J., Zhou, H., Meng, A., and Chen, Y. (2007). The evolutionally conserved activity of Dapper2 in antagonizing TGF-ß signaling. The FASEB Journal *21*, 682–690.
Sun, X., Essalmani, R., Day, R., Khatib, A.M., Seidah, N.G., and Prat, A. (2012). Proprotein convertase subtilisin/kexin type 9 deficiency reduces melanoma metastasis in liver. Neoplasia (United States) *14*, 1122–1131.
Topczewska, J.M., Postovit, L.M., Margaryan, N. V., Sam, A., Hess, A.R., Wheaton, W.W., Nickoloff, B.J., Topczewski, J., and Hendrix, M.J.C. (2006). Embryonic and tumorigenic pathways converge via Nodal signaling: Role in melanoma aggressiveness. Nature Medicine *12*, 925–932.
Tsuneyoshi, N., Sumi, T., Onda, H., Nojima, H., Nakatsuji, N., and Suemori, H. (2008). PRDM14 suppresses expression of differentiation marker genes in human embryonic stem cells. Biochem Biophys Res Commun *367*, 899–905.
Vallier, L., Mendjan, S., Brown, S., Chng, Z., Teo, A., Smithers, L.E., Trotter, M.W.B.B., Cho, C.H.H.H.-H., Martinez, A., Rugg-Gunn, P., et al. (2009). Activin/Nodal signalling maintains pluripotency by controlling Nanog expression. Development *136*, 1339–1349.
Zhang, D.W., Lagace, T.A., Garuti, R., Zhao, Z., McDonald, M., Horton, J.D., Cohen, J.C., and Hobbs, H.H. (2007). Binding of proprotein convertase subtilisin/kexin type 9 to epidermal growth factor-like repeat A of low density lipoprotein receptor decreases receptor recycling and increases degradation. Journal of Biological Chemistry *282*, 18602–18612.
Zhang, L., Zhou, H., Su, Y., Sun, Z., Zhang, H., Zhang, L., Zhang, Y., Ning, Y., Chen, Y.G., and Meng, A. (2004). Zebrafish Dpr2 inhibits mesoderm induction by promoting degradation of nodal receptors. Science *306*, 114–117.
Zhao, Z., Tuakli-Wosornu, Y., Lagace, T.A., Kinch, L., Grishin, N. V., Horton, J.D., Cohen, J.C., and Hobbs, H.H. (2006). Molecular characterization of loss-of-function mutations in PCSK9 and identification of a compound heterozygote. American Journal of Human Genetics *79*, 514–523.

FIGURE TITLES AND LEGENDS

Figure 1. PCSK9 is highly expressed in undifferentiated hiPSCs. **A.** Daily PCSK9 mRNA expression throughout hiPSC differentiation into HLCs (n=3 independent differentiations). **B.** Left Panel, PCSK9 protein expression quantification by western blot analysis in hiPSCs and hepatic progenitor cell lysates (n=3 independent differentiations). Right panel, western blot quantifications upon ß-actin normalization. **C.** Secreted PCSK9 protein quantification in cell culture supernatant by ELISA assay at day 0, 5, 10, 15 and 20 of HLCs differentiation (n=3 independent differentiations), ** p value <0.01.

Figure 2. PCSK9 inhibition impairs *NODAL* gene expression and hiPSCs proliferation. **A.** Q-PCR analysis expression of *PCSK9*, *LDLR*, *NODAL*, *LEFTY1*, *NANOG*, *OCT3/4* and *SOX2* in hiPSCs expressing a control shRNA or directed against PCSK9 (n=3 different hiPSC passages). **B.** Cell growth of hiPSCs expressing a control shRNA compared to a shRNA directed against PCSK9 (n=4 independent experiments), * p value <0.05.

Figure 3. hiPSCs proliferation and SMAD2 phosphorylation status are modulated by PCSK9 inhibition or overexpression. **A.** Left Panel, PCSK9 protein expression quantification by western blot analysis in hiPSCs knock out (n=9: 3 passages of 3 different hiPSC clones) and hiPSCs overexpressing PCSK9-FULL (n=3 different hiPSC passages). Right panel, western blot quantifications upon α-tubulin normalization. **B.** Cell growth of hiPSCs control compared to a knocked out for PCSK9 and hiPSCs overexpressing PCSK9-FULL (respectively, n=4 and n=3 independent experiments). **C.** Left Panel, P-SMAD2 and total SMAD2 detection by western blot in hiPSCs knockout for PCSK9 (n=9: 3 passages of 3 different hiPS clones) or overexpressing PCSK9-FULL (n=3 different passages) compared to hiPSCs control (n=3 different passages). Right panel, western blot quantification analyzed on the ratio P-SMAD2/total SMAD2/α-tubulin), * p value <0.05, ** p value <0.01.

Figure 4. PCSK9 loss of function mutations R104C/V114A inhibit hiPS cell proliferation and decrease SMAD2 phosphorylation. **A.** Western blot directed against PCSK9 and ß-actin in hiPSCs control (n=3 different passages) and R104C/V114A (n=3 different passages) **B.** Cell growth of hiPSCs control compared to hiPSCs carrying the PCSK9-R104C/V114A mutations (n=4 independent experiments). **C.** Left Panel, P-SMAD2 and total SMAD2 detection by western blot in hiPSCs control (n=3 different passages) and R104C/V114A (n=3

different passages). Right panel, western blot quantification analyzed on the ratio P-SMAD2/T-SMAD2/α-tubulin. **D.** TGFß-promoter activity detection by luciferase assay in control hiPSCs (n=3 different passages) and hiPSCs carrying the R104C/V114A mutations (n=3 different passages). * p value <0.05, *** p value <0.001.

Figure 5. PCSK9 regulates the abundance of the TGFßR1 at the cell membrane. A. Protein detection by western blot of the transferrin receptor, the TGFß-R1 receptor and GAPDH in hiPSCs total lysate (left panel) or at the cell membrane upon biotinylation assay (middle panel) quantified as a ratio of TGFß-R1/Transferrin receptor (right panel). * p value < 0,05

Figure 6. PCSK9 is acting intracellularly through DACT2. A. Left panel, DACT2 detection by western blot in control (n=3 different passages), PCSK9-KO (n=9, 3 passages of 3 different hiPSC clones) hiPS cell lines. Right panel, western blot quantifications upon α-tubulin normalization; **B.** Left panel, DACT2 detection by western blot in control (n=3 different passages) and PCSK9-R104C/V114A (n=3 different passages) hiPS cell lines. Right panel, western blot quantifications upon α-tubulin normalization; **C.** Left panel, DACT2 detection by western blot in control (n=3 different passages) and PCSK9-FULL overexpression (n=3 different passages) hiPS cell lines. Right panel, western blot quantifications upon α-tubulin normalization; * p value <0.05, ns: non-significant.

Figure 7. PCSK9 is interacting with DACT2 through its CHRD domain. A. Diagram picturing the different V5-PCSK9 constructs tested. **B.** V5-PCSK9 and DACT2 detection by western blot upon V5 co-immunoprecipitation in cellular lysate of hiPS cells expressing the FULL-PCSK9, L455X or CHRD construct. Immunoglobulin (Ig) was used as a negative control while V5 directed antibody was to pull down FULL-PCSK9, L455X or CHRD.

A

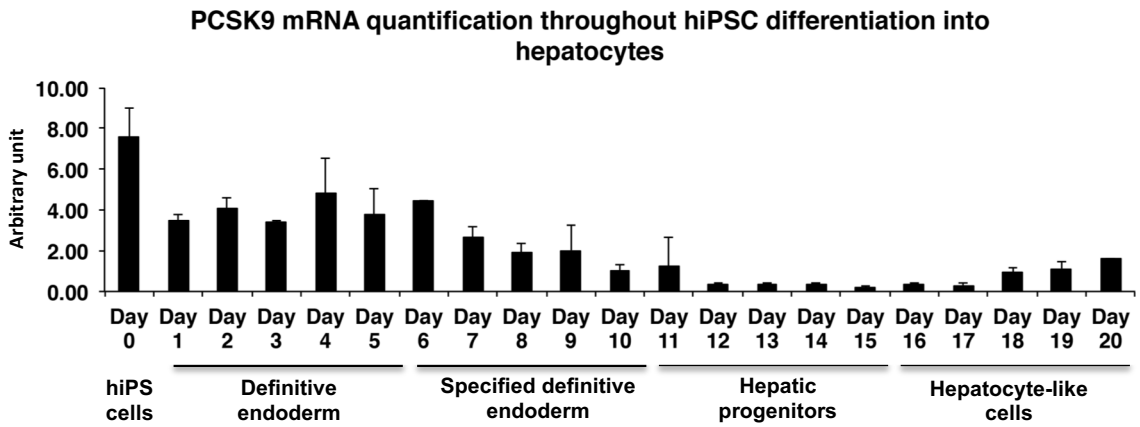
PCSK9 mRNA quantification throughout hiPSC differentiation into hepatocytes
Arbitrary unit
10.00
8.00
6.00
4.00
2.00
0.00
Day 0
Day 1
Day 2
Day 3
Day 4
Day 5
Day 6
Day 7
Day 8
Day 9
Day 10
Day 11
Day 12
Day 13
Day 14
Day 15
Day 16
Day 17
Day 18
Day 19
Day 20
hiPS cells
Definitive endoderm
Specified definitive endoderm
Hepatic progenitors
Hepatocyte-like cells

B

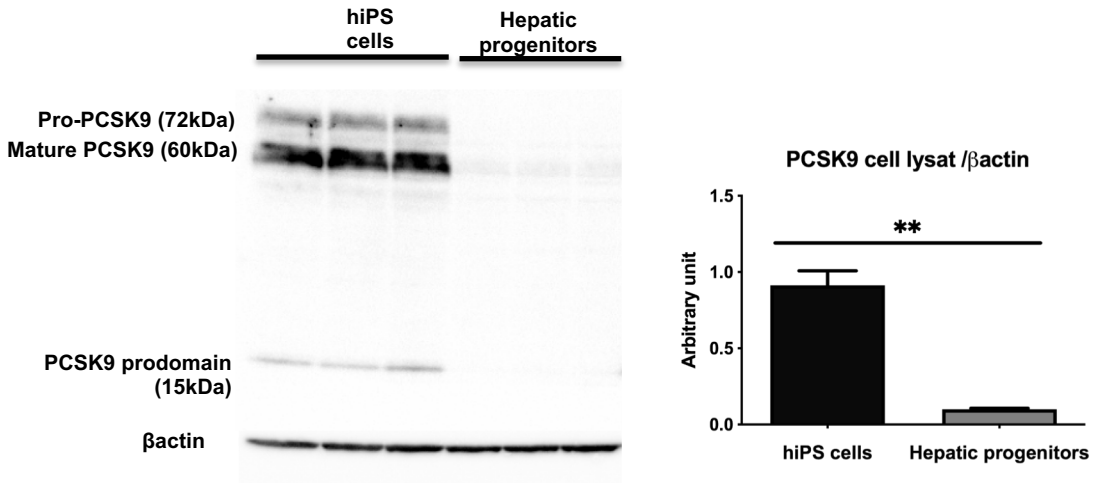
hiPS cells
Hepatic progenitors
Pro-PCSK9 (72kDa)
Mature PCSK9 (60kDa)
PCSK9 prodomain (15kDa)
βactin
PCSK9 cell lysat /βactin
Arbitrary unit
1.5
1.0
0.5
0.0
**
hiPS cells
Hepatic progenitors

C

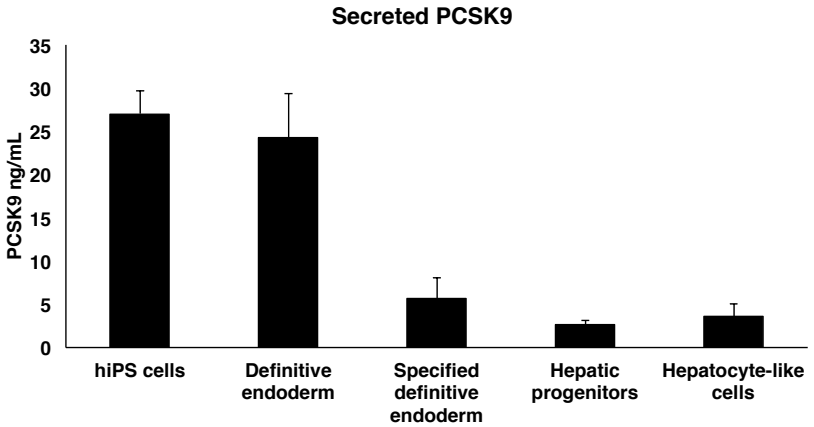
Secreted PCSK9
PCSK9 ng/mL
35
30
25
20
15
10
5
0
hiPS cells
Definitive endoderm
Specified definitive endoderm
Hepatic progenitors
Hepatocyte-like cells

Figure 1

A

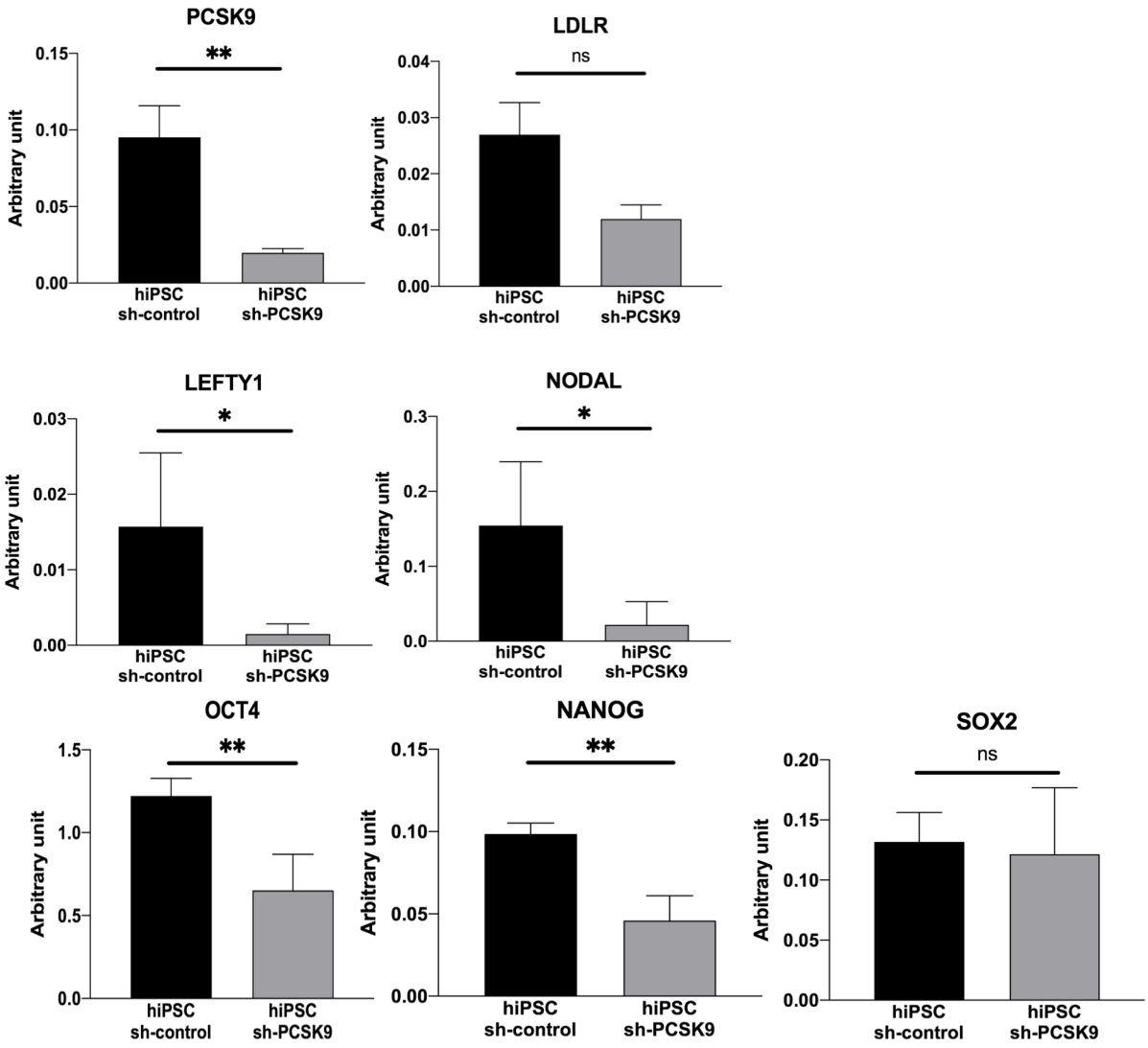
PCSK9
**
Arbitrary unit
0.15
0.10
0.05
0.00
hiPSC sh-control
hiPSC sh-PCSK9
LDLR
ns
0.04
0.03
0.02
0.01
0.00
LEFTY1
*
0.03
0.02
0.01
0.00
NODAL
*
0.3
0.2
0.1
0.0
OCT4
**
1.5
1.0
0.5
0.0
NANOG
**
0.15
0.10
0.05
0.00
SOX2
ns
0.20
0.15
0.10
0.05
0.00

B

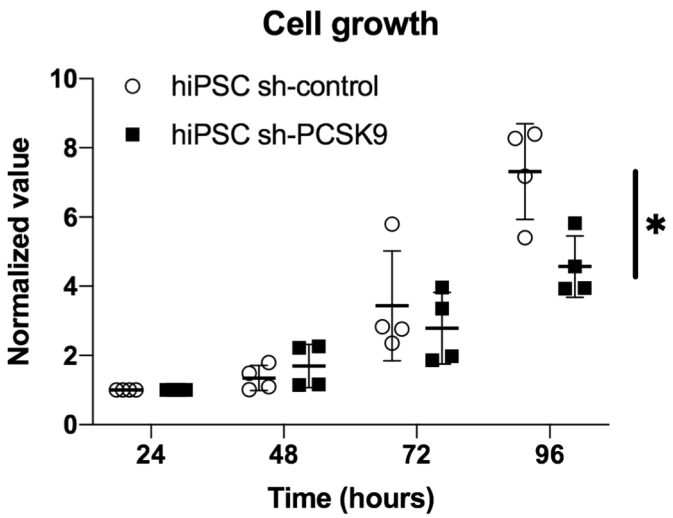
Cell growth
hiPSC sh-control
hiPSC sh-PCSK9
Normalized value
10
8
6
4
2
0
24
48
72
96
Time (hours)
*

Figure 2

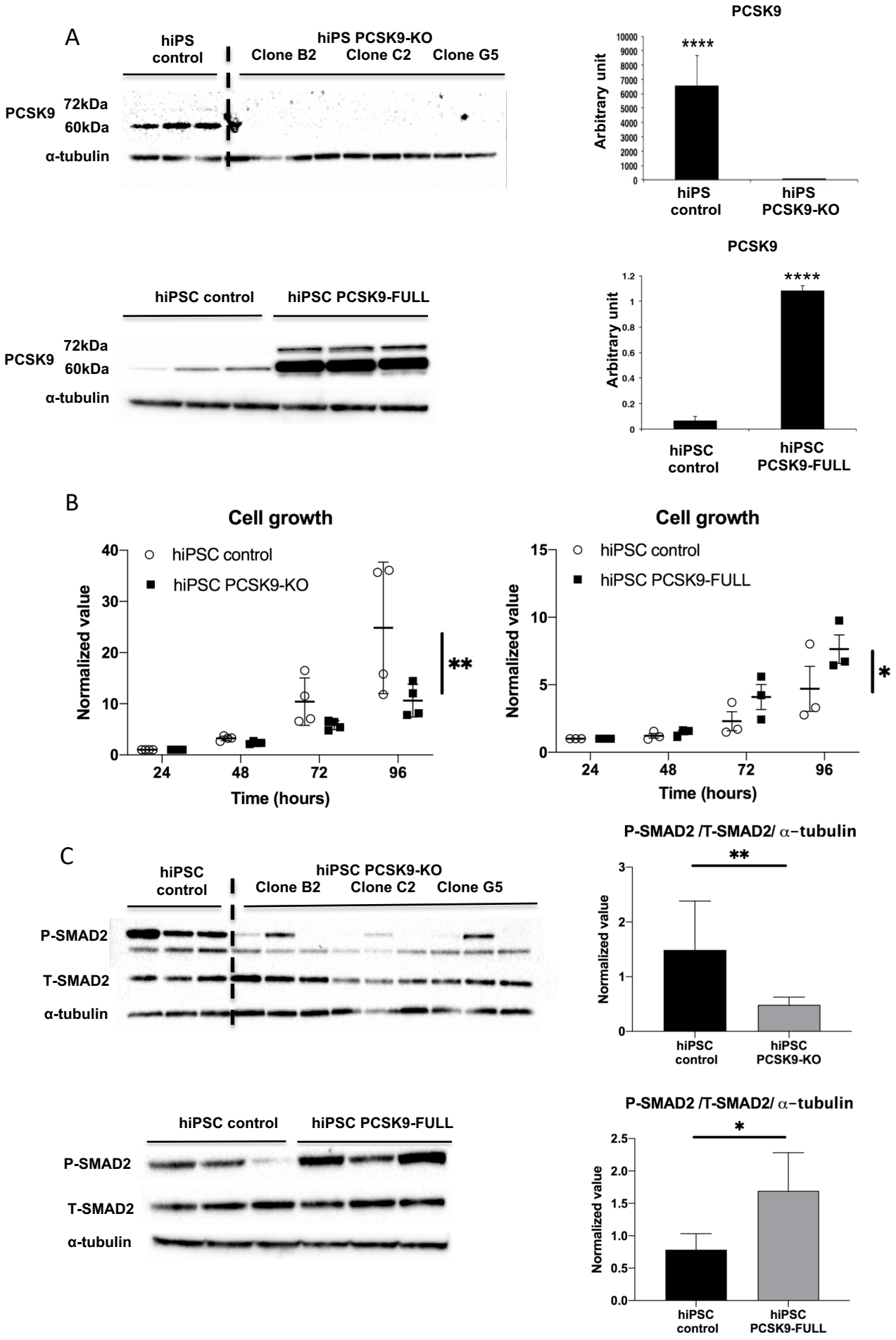
A
hiPS control
hiPS PCSK9-KO
Clone B2
Clone C2
Clone G5
PCSK9
72kDa
60kDa
α-tubulin
PCSK9
Arbitrary unit
****
hiPS control
hiPS PCSK9-KO
hiPSC control
hiPSC PCSK9-FULL
PCSK9
72kDa
60kDa
α-tubulin
PCSK9
Arbitrary unit
****
hiPSC control
hiPSC PCSK9-FULL
B
Cell growth
hiPSC control
hiPSC PCSK9-KO
Normalized value
Time (hours)
**
Cell growth
hiPSC control
hiPSC PCSK9-FULL
Normalized value
Time (hours)
*
C
hiPSC control
hiPSC PCSK9-KO
Clone B2
Clone C2
Clone G5
P-SMAD2
T-SMAD2
α-tubulin
P-SMAD2 /T-SMAD2/ α−tubulin
**
Normalized value
hiPSC control
hiPSC PCSK9-KO
hiPSC control
hiPSC PCSK9-FULL
P-SMAD2
T-SMAD2
α-tubulin
P-SMAD2 /T-SMAD2/ α−tubulin
*
Normalized value
hiPSC control
hiPSC PCSK9-FULL

Figure 3

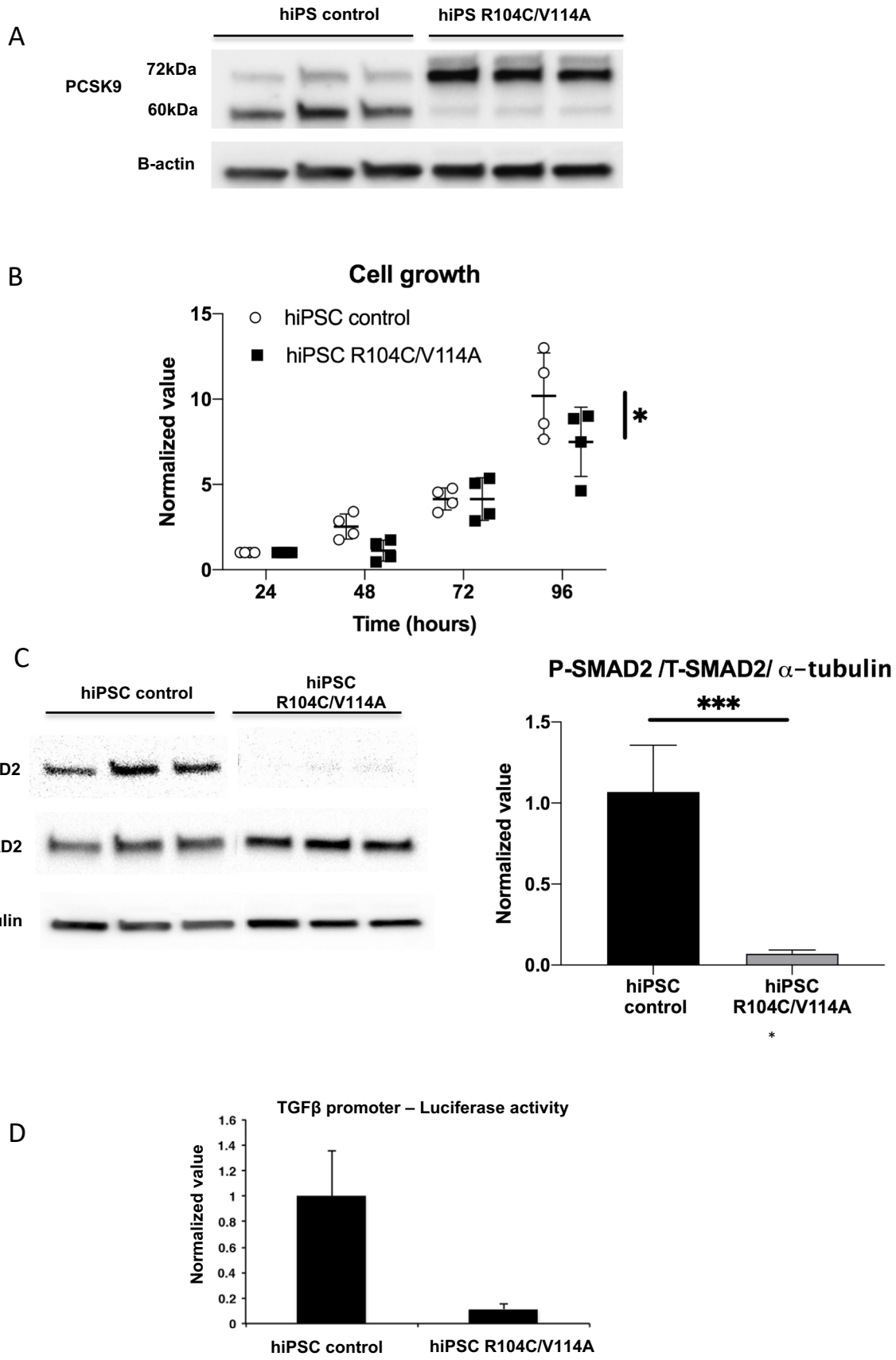
A
hiPS control
hiPS R104C/V114A
PCSK9
72kDa
60kDa
B-actin
B
Cell growth
hiPSC control
hiPSC R104C/V114A
Normalized value
15
10
5
0
24
48
72
96
Time (hours)
*
C
hiPSC control
hiPSC R104C/V114A
P-SMAD2
T-SMAD2
α-tubulin
P-SMAD2 /T-SMAD2/ α−tubulin
***
Normalized value
1.5
1.0
0.5
0.0
hiPSC control
hiPSC R104C/V114A
*
D
TGFβ promoter – Luciferase activity
Normalized value
1.6
1.4
1.2
1
0.8
0.6
0.4
0.2
0
hiPSC control
hiPSC R104C/V114A

Figure 4

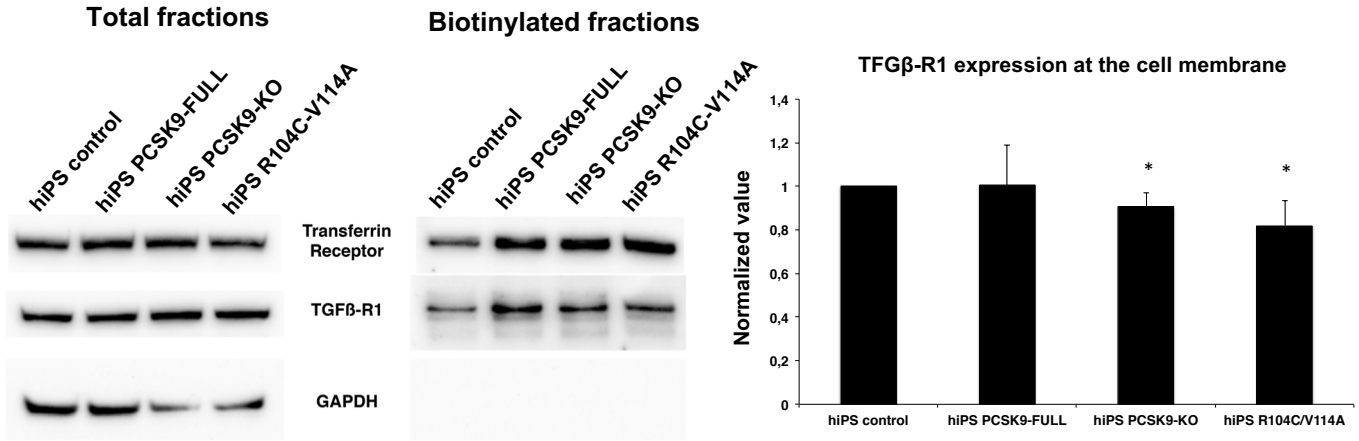
Total fractions
Biotinylated fractions
hiPS control
hiPS PCSK9-FULL
hiPS PCSK9-KO
hiPS R104C-V114A
Transferrin Receptor
TGFß-R1
GAPDH
TFGβ-R1 expression at the cell membrane
Normalized value
1,4
1,2
1
0,8
0,6
0,4
0,2
0
*
*
hiPS control
hiPS PCSK9-FULL
hiPS PCSK9-KO
hiPS R104C/V114A

Figure 5

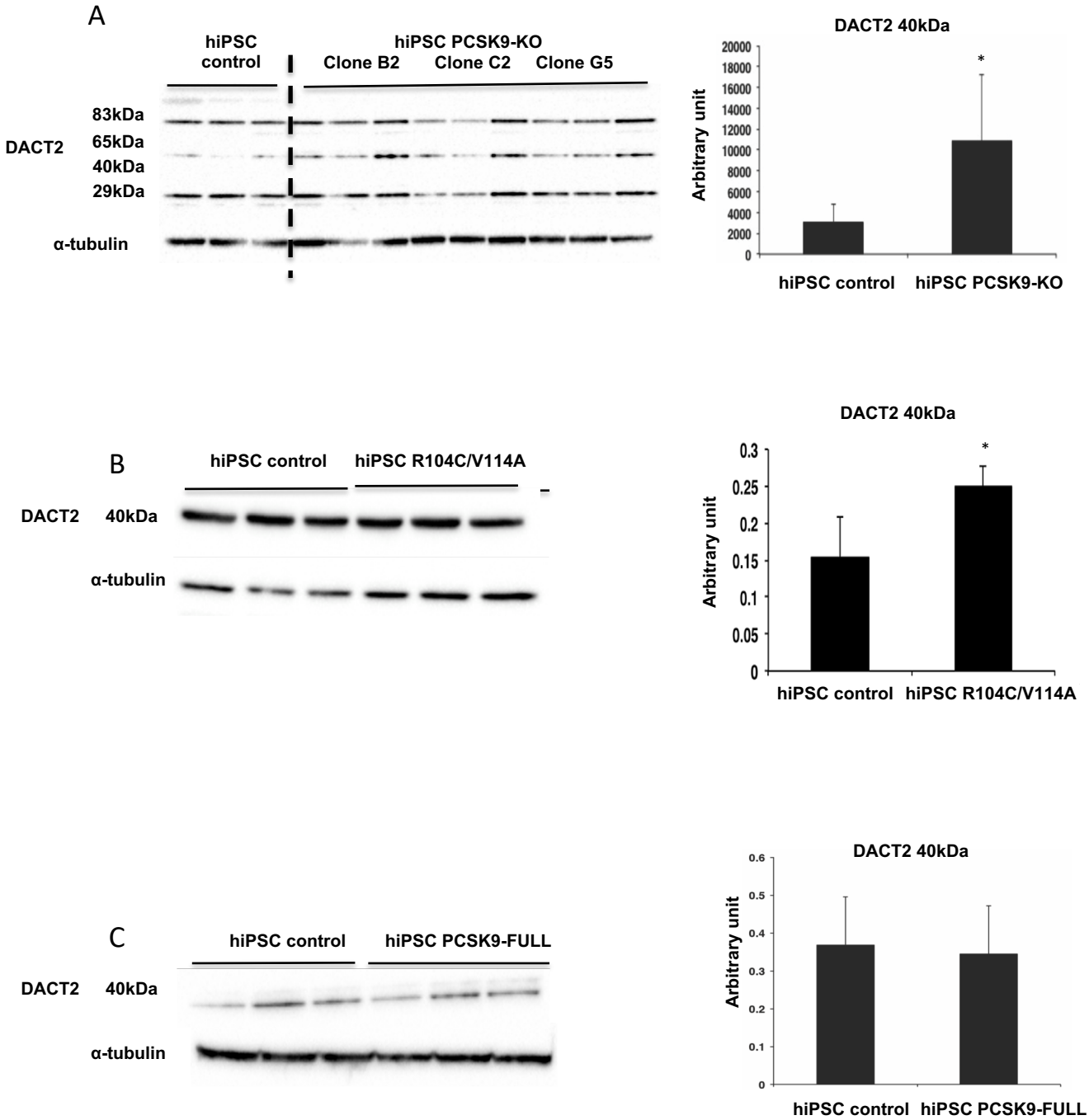
A
hiPSC control
hiPSC PCSK9-KO
Clone B2
Clone C2
Clone G5
83kDa
65kDa
40kDa
29kDa
DACT2
α-tubulin
DACT2 40kDa
Arbitrary unit
20000
18000
16000
14000
12000
10000
8000
6000
4000
2000
0
*
hiPSC control
hiPSC PCSK9-KO
B
hiPSC control
hiPSC R104C/V114A
DACT2
40kDa
α-tubulin
DACT2 40kDa
Arbitrary unit
0.3
0.25
0.2
0.15
0.1
0.05
0
*
hiPSC control
hiPSC R104C/V114A
C
hiPSC control
hiPSC PCSK9-FULL
DACT2
40kDa
α-tubulin
DACT2 40kDa
Arbitrary unit
0.6
0.5
0.4
0.3
0.2
0.1
0
hiPSC control
hiPSC PCSK9-FULL

Figure 6

A

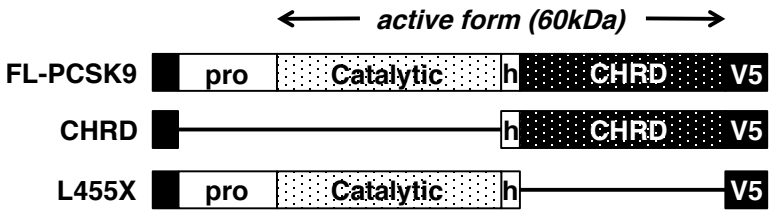
active form (60kDa)
FL-PCSK9
pro
Catalytic
h
CHRD
V5
CHRD
h
CHRD
V5
L455X
pro
Catalytic
h
V5

B

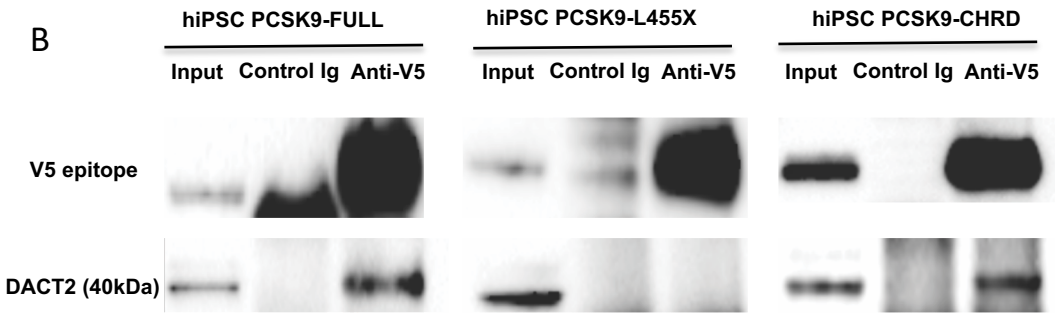
hiPSC PCSK9-FULL
hiPSC PCSK9-L455X
hiPSC PCSK9-CHRD
Input
Control Ig
Anti-V5
Input
Control Ig
Anti-V5
Input
Control Ig
Anti-V5
V5 epitope
DACT2 (40kDa)

Figure 7